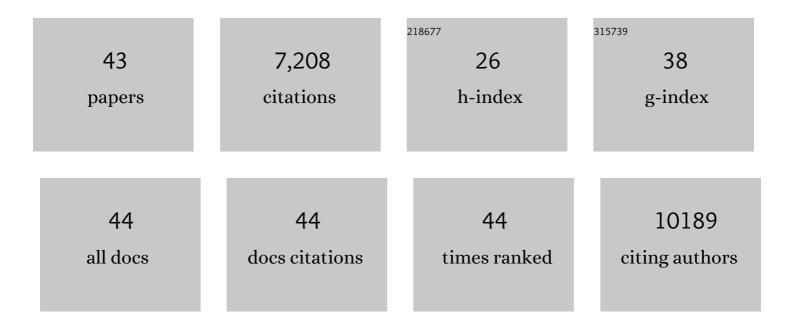
Michael E Oskin

List of Publications by Year in descending order

Source: https://exaly.com/author-pdf/5569255/publications.pdf Version: 2024-02-01



#	Article	IF	CITATIONS
1	The Shuttle Radar Topography Mission. Reviews of Geophysics, 2007, 45, .	23.0	5,113
2	Effects of bedrock landslides on cosmogenically determined erosion rates. Earth and Planetary Science Letters, 2005, 237, 480-498.	4.4	242
3	Near-Field Deformation from the El Mayor–Cucapah Earthquake Revealed by Differential LIDAR. Science, 2012, 335, 702-705.	12.6	206
4	Exhumation of basement-cored uplifts: Example of the Kyrgyz Range quantified with apatite fission track thermochronology. Tectonics, 2006, 25, n/a-n/a.	2.8	129
5	Assembly of a large earthquake from a complex fault system: Surface rupture kinematics of the 4 April 2010 El Mayor–Cucapah (Mexico) Mw 7.2 earthquake. , 2014, 10, 797-827.		127
6	Pulsed exhumation of interior eastern Tibet: Implications for relief generation mechanisms and the origin of high-elevation planation surfaces. Earth and Planetary Science Letters, 2016, 449, 176-185.	4.4	100
7	Alpine landscape evolution dominated by cirque retreat. Geology, 2005, 33, 933.	4.4	94
8	Coseismic fault zone deformation revealed with differential lidar: Examples from Japanese <mml:math xmlns:mml="http://www.w3.org/1998/Math/MathML" altimg="si1.gif" overflow="scroll"><mml:msub><mml:mrow><mml:mi mathvariant="normal">M</mml:mi </mml:mrow><mml:mrow><mml:mi>w</mml:mi>intraplate earthquakes. Earth and Planetary Science Letters, 2014, 405, 244-256.</mml:mrow></mml:msub></mml:math 	4.4 > <td>83 ath>â^1⁄47</td>	83 ath>â^1⁄47
9	Rupture termination at restraining bends: The last great earthquake on the Altyn Tagh Fault. Geophysical Research Letters, 2015, 42, 2164-2170.	4.0	63
10	Inherited strikeâ€slip faults as an origin for basementâ€cored uplifts: Example of the Kungey and Zailiskey ranges, northern Tian Shan. Tectonics, 2012, 31, .	2.8	61
11	Deformation processes adjacent to active faults: Examples from eastern California. Journal of Geophysical Research, 2010, 115, .	3.3	60
12	Coseismic slip variation assessed from terrestrial lidar scans of the El Mayor–Cucapah surface rupture. Earth and Planetary Science Letters, 2013, 366, 151-162.	4.4	60
13	The role of a keystone fault in triggering the complex El Mayor–Cucapah earthquake rupture. Nature Geoscience, 2016, 9, 303-307.	12.9	60
14	Late Quaternary slip rate gradient defined using highâ€resolution topography and ¹⁰ Be dating of offset landforms on the southern San Jacinto Fault zone, California. Journal of Geophysical Research, 2010, 115, .	3.3	56
15	Geologic and structural controls on rupture zone fabric: A field-based study of the 2010 Mw 7.2 El Mayor-Cucapah earthquake surface rupture. , 2015, 11, 899-920.		52
16	Focused modern denudation of the Longmen Shan margin, eastern Tibetan Plateau. Geochemistry, Geophysics, Geosystems, 2011, 12, n/a-n/a.	2.5	51
17	Optimization of legacy lidar data sets for measuring nearâ€field earthquake displacements. Geophysical Research Letters, 2014, 41, 3494-3501.	4.0	47
18	Documentation of Surface Fault Rupture and Ground-Deformation Features Produced by the 4 and 5 July 2019 MwÂ6.4 and MwÂ7.1 Ridgecrest Earthquake Sequence. Seismological Research Letters, 2020, 91, 2942-2959.	1.9	47

MICHAEL E OSKIN

#	Article	IF	CITATIONS
19	Thick deltaic sedimentation and detachment faulting delay the onset of continental rupture in the Northern Gulf of California: Analysis of seismic reflection profiles. Tectonics, 2013, 32, 1294-1311.	2.8	41
20	Transient landscape evolution of basement ored uplifts: Example of the Kyrgyz Range, Tian Shan. Journal of Geophysical Research, 2007, 112, .	3.3	40
21	Topographic control of asynchronous glacial advances: A case study from Annapurna, Nepal. Geophysical Research Letters, 2011, 38, n/a-n/a.	4.0	38
22	Palinspastic restoration of NAVDat and implications for the origin of magmatism in southwestern North America. Journal of Geophysical Research, 2010, 115, .	3.3	37
23	Reevaluation of the Late Pleistocene Slip Rate of the Haiyuan Fault Near Songshan, Gansu Province, China. Journal of Geophysical Research: Solid Earth, 2019, 124, 5217-5240.	3.4	35
24	Structure and geometry of the Aksay restraining double bend along the Altyn Tagh Fault, northern Tibet, imaged using magnetotelluric method. Geophysical Research Letters, 2017, 44, 4090-4097.	4.0	34
25	A 6000-year-long paleoseismologic record of earthquakes along the Xorkoli section of the Altyn Tagh fault, China. Earth and Planetary Science Letters, 2018, 497, 193-203.	4.4	34
26	Eastern termination of the Altyn Tagh Fault, western China: Constraints from a magnetotelluric survey. Journal of Geophysical Research: Solid Earth, 2015, 120, 2838-2858.	3.4	32
27	Airborne Lidar and Electro-Optical Imagery along Surface Ruptures of the 2019 Ridgecrest Earthquake Sequence, Southern California. Seismological Research Letters, 2020, 91, 2096-2107.	1.9	31
28	Geomorphic offsets along the creeping Laohu Shan section of the Haiyuan fault, northern Tibetan Plateau. , 2018, 14, 1165-1186.		30
29	Stable, rapid rate of slip since inception of the San Jacinto fault, California. Geophysical Research Letters, 2013, 40, 4209-4213.	4.0	29
30	Accrual of widespread rock damage from the 2019 Ridgecrest earthquakes. Nature Geoscience, 2022, 15, 222-226.	12.9	23
31	Paleoseismic Investigation of the Aksay Restraining Double Bend, Altyn Tagh Fault, and Its Implication for Barrierâ€Breaching Ruptures. Journal of Geophysical Research: Solid Earth, 2018, 123, 4307-4330.	3.4	20
32	Late Pleistocene slip rate of the central Haiyuan fault constrained from optically stimulated luminescence, 14C, and cosmogenic isotope dating and high-resolution topography. Bulletin of the Geological Society of America, 2021, 133, 1347-1369.	3.3	18
33	Characteristic slip distribution and earthquake recurrence along the eastern Altyn Tagh fault revealed by high-resolution topographic data. , 2020, 16, 392-406.		16
34	An analysis of the factors that control fault zone architecture and the importance of fault orientation relative to regional stress. Bulletin of the Geological Society of America, 2020, 132, 2084-2104.	3.3	14
35	Point-based computing on scanned terrain with LidarViewer. , 2013, 9, 546-556.		12
36	Surfaceâ€Rupture and Slip Observations on the Day of the 24 August 2014 South Napa Earthquake. Seismological Research Letters, 2015, 86, 1119-1127.	1.9	12

MICHAEL E OSKIN

#	Article	IF	CITATIONS
37	Segmented Thrust Faulting: Example From the Northeastern Margin of the Tibetan Plateau. Journal of Geophysical Research: Solid Earth, 2020, 125, e2019JB018634.	3.4	11
38	Surface Slip From the 2014 South Napa Earthquake Measured With Structure From Motion and $3\hat{e} \Theta$ Virtual Reality. Geophysical Research Letters, 2018, 45, 5985-5991.	4.0	9
39	Extent of Lowâ€Angle Normal Slip in the 2010 El Mayorâ€Cucapah (Mexico) Earthquake From Differential Lidar. Journal of Geophysical Research: Solid Earth, 2019, 124, 943-956.	3.4	9
40	Near-Field High-Resolution Maps of the Ridgecrest Earthquakes from Aerial Imagery. Seismological Research Letters, 2022, 93, 494-499.	1.9	9
41	Southern California Earthquake Center Geologic Vertical Motion Database. Geochemistry, Geophysics, Geosystems, 2008, 9, .	2.5	8
42	Steady ¹⁰ Beâ€derived paleoerosion rates across the Plioâ€Pleistocene climate transition, Fish Creekâ€Vallecito basin, California. Journal of Geophysical Research F: Earth Surface, 2017, 122, 1653-1677.	2.8	8
43	Relationship of channel steepness to channel incision rate from a tilted and progressively exposed unconformity surface. Journal of Geophysical Research F: Earth Surface, 2014, 119, 366-384.	2.8	7